Article

Developmental Cell

Control of Cell Shape, Neurite Outgrowth, and Migration by a Nogo-A/HSPG Interaction

Graphical Abstract

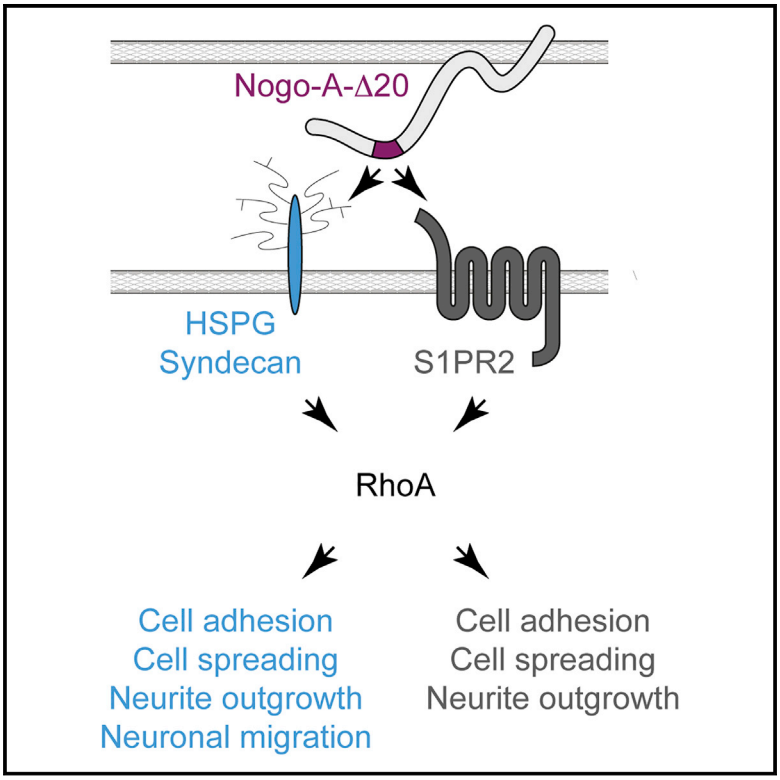

Authors

Anissa Kempf, Enrica Boda, Jessica C.F. Kwok, ..., Olivier Pertz, Annalisa Buffo, Martin E. Schwab

Correspondence

anissa.kempf@cncb.ox.ac.uk (A.K.), schwab@hifo.uzh.ch (M.E.S.)

In Brief

The extracellular Δ20 domain of Nogo-A is a potent inhibitor of cell adhesion and neurite outgrowth in the adult CNS. Kempf et al. identify HSPGs as functional receptors for Nogo-A-Δ20. Nogo-A-Δ20 binds to HSPGs and regulates RhoA activation, cell spreading, neurite outgrowth, and neuroblast migration via HSPGs.

Highlights

- Nogo-A-Δ20 inhibits cell spreading and neurite outgrowth via HSPGs
- Nogo-A-Δ20 binds HSPGs and activates RhoA via HSPGs
- The HSPG family members Sdc3 and Sdc4 are required for Nogo-A-Δ20 inhibition
- Nogo-A-Δ20 regulates neuroblast migration via HSPGs but independently of S1PR2

Kempf et al., 2017, Developmental Cell *43*, 24–34
October 9, 2017
http://dx.doi.org/10.1016/j.devcel.2017.08.014

CellPress

CellPress

Developmental Cell
Article

Control of Cell Shape, Neurite Outgrowth, and Migration by a Nogo-A/HSPG Interaction

Anissa Kempf,[1,6,9,*] Enrica Boda,[2] Jessica C.F. Kwok,[3,8] Rafael Fritz,[4] Valentina Grande,[2] Andrea M. Kaelin,[1] Zorica Ristic,[1] Andre Schmandke,[1] Antonio Schmandke,[1] Bjoern Tews,[5] James W. Fawcett,[3] Olivier Pertz,[4,7] Annalisa Buffo,[2] and Martin E. Schwab[1,*]

[1]Brain Research Institute, University of Zurich and Department of Health Sciences and Technology, Swiss Federal Institute of Technology (ETH) Zurich, 8057 Zurich, Switzerland

[2]Department of Neuroscience, Neuroscience Institute Cavalieri Ottolenghi (NICO), Università degli Studi di Torino, Orbassano, Turin 10043, Italy

[3]John van Geest Centre for Brain Repair, Department of Clinical Neurosciences, University of Cambridge, Robinson Way, Cambridge CB2 0PY, UK

[4]Institute for Biochemistry and Genetics, Department of Biomedicine, University of Basel, 4058 Basel, Switzerland

[5]Schaller Research Group at the University of Heidelberg and the German Cancer Research Center (DKFZ), Molecular Mechanisms of Tumor Invasion, 69120 Heidelberg, Germany

[6]Present address: University of Oxford, Centre for Neural Circuits and Behaviour, Oxford OX1 3SR, UK

[7]Present address: Institute of Cell Biology, University of Bern, Bern 3012, Switzerland

[8]Present address: School of Biomedical Sciences, Faculty of Biological Sciences, University of Leeds, Leeds LS2 9JT, UK

[9]Lead Contact

*Correspondence: anissa.kempf@cncb.ox.ac.uk (A.K.), schwab@hifo.uzh.ch (M.E.S.)

http://dx.doi.org/10.1016/j.devcel.2017.08.014

SUMMARY

Heparan sulfate proteoglycans (HSPGs) critically modulate adhesion-, growth-, and migration-related processes. Here, we show that the transmembrane protein, Nogo-A, inhibits neurite outgrowth and cell spreading in neurons and Nogo-A-responsive cell lines via HSPGs. The extracellular, active 180 amino acid Nogo-A region, named Nogo-A-Δ20, binds to heparin and brain-derived heparan sulfate glycosaminoglycans (GAGs) but not to the closely related chondroitin sulfate GAGs. HSPGs are required for Nogo-A-Δ20-induced inhibition of adhesion, cell spreading, and neurite outgrowth, as well as for RhoA activation. Surprisingly, we show that Nogo-A-Δ20 can act via HSPGs independently of its receptor, Sphingosine-1-Phosphate receptor 2 (S1PR2). We thereby identify the HSPG family members syndecan-3 and syndecan-4 as functional receptors for Nogo-A-Δ20. Finally, we show in explant cultures *ex vivo* that Nogo-A-Δ20 promotes the migration of neuroblasts via HSPGs but not S1PR2.

INTRODUCTION

Cell-surface heparan sulfate proteoglycans (HSPGs) are highly expressed in the mammalian nervous system (Sarrazin et al., 2011; Yamaguchi, 2001). HSPGs regulate various developmental processes ranging from neuroblast migration, axon growth, and guidance to synapse formation and neuronal connectivity (Inatani et al., 2003; Van Vactor et al., 2006; Yamaguchi, 2001). HSPGs transduce signals originating in the extracellular matrix (ECM) or act as obligate co-receptors for several morphogens, growth factors, and axon guidance molecules (Bernfield et al., 1999; Sarrazin et al., 2011). Most studies of HSPGs have focused on the regulation of survival-, proliferation-, or growth-promoting cues, e.g., fibroblast growth factor (FGF) (Sarrazin et al., 2011), rather than growth-inhibiting and repulsive factors. To our knowledge, only the repulsive activities of EphrinA3, Slit2, and S1P have been reported to critically depend on the presence of cell-surface HSPGs (Hu, 2001; Irie et al., 2008; Strochlic et al., 2008).

Nogo-A is a major anti-adhesive and neurite growth-inhibitory protein initially discovered for its role as a myelin-associated inhibitor of axonal regeneration in the adult CNS (Schwab, 2010). In addition to its role in the injured CNS, Nogo-A has been shown to regulate various developmental and plastic processes ranging from synapse formation to neuronal migration (Kempf and Schwab, 2013; Schwab and Strittmatter, 2014). In the adult brain, Nogo-A promotes cell motility and the tangential migration of neuroblasts along the rostral migratory stream (RMS) by triggering cell-cell repulsion (Rolando et al., 2012). At hippocampal and cortical synapses, Nogo-A acts as a negative regulator of long-term potentiation and memory stability (Karlsson et al., 2016; Schwab and Strittmatter, 2014). However, it is not known if Nogo-A-evoked cellular responses are modulated by HSPGs.

In this study, we identified HSPGs as functional receptors for the active Nogo-A domain, Nogo-A-Δ20 (rat amino acid [aa] 544–725) (Oertle et al., 2003). We found that Nogo-A-Δ20 activates RhoA and inhibits cell spreading and neurite outgrowth via HSPGs, specifically via the transmembrane HSPGs, syndecan-3 and syndecan-4. In addition, we show that Nogo-A-Δ20 inhibits cell adhesion of neuroblasts in an HSPG-dependent manner and increases neuroblast chain

migration *ex vivo*. Our results propose a mechanism by which Nogo-A-Δ20 affects cytoskeletal dynamics by interacting with HSPGs independently of the previously characterized Nogo-A-Δ20 receptor, Sphingosine-1-Phosphate receptor 2 (S1PR2) (Kempf et al., 2014).

RESULTS

Cell-Surface Heparan Sulfate Is Required for Nogo-A-Δ20-Induced Inhibition of Cell Spreading

Outgrowth of neurites and spreading of cells, e.g., fibroblasts, are strongly inhibited by substrates containing Nogo-A or its active fragment, Nogo-A-Δ20 (Oertle et al., 2003) (Figure 1A). To determine a possible role of heparan sulfate (HS), cell-spreading inhibition was examined upon enzymatic cleavage of HS. Treatment of Swiss 3T3 cells with heparinase III (HepIII) significantly increased cell spreading by ~45% on the Nogo-A-Δ20-coated culture dishes when compared with the vehicle (saline) control (Figures 1A and 1B). Treatment with heparinase I (HepI), which cleaves HS at the level of *O*-sulfated rather than non-sulfated or *N*-sulfated disaccharides (Hovingh and Linker, 1970), resulted in a similar decrease of the Nogo-A-Δ20 inhibition but required higher enzyme concentrations (Figure S1A).

If endogenous HS promotes the Nogo-A-Δ20 inhibitory effects by directly binding to Nogo-A, excess soluble HS in the culture medium may act as competitive inhibitor and neutralize Nogo-A-mediated cell-spreading inhibition. Indeed, acute application of exogenous HS significantly increased cell spreading on a Nogo-A-Δ20 substrate when compared with control treatment (Figures 1A and 1C). Similar effects were also observed when HS was added to Nogo-A-Δ20-coated plates and washed prior to plating the cells, suggesting that Nogo-A-Δ20-bound HS neutralizes cell-spreading inhibition (Figure S1B).

To confirm the involvement of HS in Nogo-A-Δ20 signaling, an HS-deficient mutant CHO cell line, pgsD-677 (Lidholt et al., 1992), was examined. Due to a mutation in the *Ext1* gene encoding for a glycosyltransferase responsible for HS polymerization, pgsD-677 cells do not produce HS (Lidholt et al., 1992). Whereas wild-type (WT) CHO cells were strongly inhibited in spreading by Nogo-A-Δ20, spreading inhibition was almost fully abolished in the HSPG-deficient pgsD-677 cells (Figures 1D and 1E). To confirm that these results are effectively due to the lack of HS, we analyzed cell spreading upon re-expression of *Ext1* in pgsD-677 cells. Indeed, *Ext1* re-expression fully restored Nogo-A-Δ20-mediated cell-spreading inhibition (Figures 1D and 1F). Flow cytometry analysis of cell-surface expression of HSPGs confirmed their absence in pgsD-677 cells and their restoration after *Ext1* re-expression, as well as their partial reduction after HepIII treatment of 3T3 cells (Figure 1G).

Cell-Surface Heparan Sulfate Is Required for Nogo-A-Δ20-Induced Inhibition of Neurite Outgrowth

We examined the functional role of HS in Nogo-A-Δ20-mediated inhibition of neurite outgrowth using postnatal day (P) 5–8 mouse cerebellar granule neurons (CGNs) as a neuronal model system. Notably, CGNs would not adhere if HepIII was applied acutely. Instead, HepIII was applied 12 hr after plating for a total duration of 24 hr. Delayed treatment of CGNs with HepIII fully abolished the growth-inhibitory effect of Nogo-A-Δ20; neurite outgrowth was increased by ~92% when compared with the saline control (Figures 2A and 2B).

To extend these findings to other neuronal populations, we analyzed the effect of HepIII treatment in postnatal dorsal root ganglion (DRG) neurons and embryonic (E19) cortical neurons. Similar to CGNs, HepIII treatment fully abolished Nogo-A-Δ20-induced inhibition of neurite outgrowth in DRG (Figures 2C and 2D) and cortical neurons (Figures 2E and 2F). Together, these results provide strong evidence for the requirement of HS chains on the surface of Nogo-A-responsive cells to promote Nogo-A-Δ20-mediated inhibition of neurite outgrowth.

Nogo-A-Δ20 Binds Heparan Sulfate and Brain-Derived Glycosaminoglycans

To investigate a possible direct binding of Nogo-A-Δ20 to HS, we used an ELISA assay. Biotinylated preparations of HS and heparin, a highly sulfated form of HS (Bernfield et al., 1999), were immobilized and tested for T7-tagged Nogo-A-Δ20 binding using two different antibodies: an anti-T7 tag and a Nogo-A-specific antibody targeting the Δ20 domain (11c7) (Oertle et al., 2003). To assess the binding specificity of Nogo-A-Δ20 to HS, three different variants of chondroitin sulfate (CS), another form of glycosaminoglycans (GAGs), were tested in parallel (CS-A, CS-C, and CS-E). In addition, another inhibitory domain of Nogo-A, Nogo-66 (rat aa 1,026–1,091), which is known to interact with a different receptor complex (Kempf and Schwab, 2013), was tested. Importantly, Nogo-66 inhibits neurite outgrowth but not cell spreading (Kempf and Schwab, 2013). Recombinant Nogo-66-Fc was detected using an Fc-specific antibody. Nogo-A-Δ20 but not Nogo-66 showed very strong binding to HS and to heparin and significantly less to CS-A, CS-C, or CS-E ($p < 0.001$) (Figure 3A). These results were replicated using GAGs extracted from adult rat brains (total GAGs) treated with HepI/III or chondroitinase ABC (ChABC) to obtain CS-containing GAGs (CS-GAGs) or HS-containing GAGs (HS-GAGs), respectively. Consistent with the above results, Nogo-A-Δ20 bound total GAGs and HS-GAGs very strongly and showed significantly less binding to CS-GAGs ($p < 0.001$) (Figure 3B). No binding of Nogo-66 to total GAGs, HS-GAGs, or CS-GAGs was observed (Figure 3B). In order to determine the specificity of the binding of Nogo-A-Δ20 to CS-GAGs, we tested the binding of the control protein, Nogo-A-Δ21 (rat aa 812–918) (Oertle et al., 2003), to brain-derived GAGs. Nogo-A-Δ21 lacks inhibitory activity but is purified under identical conditions. No difference in binding was observed between Nogo-A-Δ21, total GAGs, HS-GAGs, or CS-GAGs (Figure S2). Moreover, the absorbance values lie in the same range as those of Nogo-A-Δ20 binding to CS-GAGs, suggesting that the binding of Nogo-A-Δ20 to CS-GAGs is likely to be non-specific. Given the fact that the results in Figures 3B and S2 are standardized against the total GAGs and that the HS:CS ratio in the brain is 1:10 (Deepa et al., 2006), Nogo-A-Δ20 shows a strong binding preference to HS-GAGs. Together, these results indicate that the key and main binding partner of Nogo-A-Δ20 is HS.

Finally, to determine the binding affinity of Nogo-A-Δ20 to heparin or HS-GAGs, a dose-response binding curve was produced (Figures 3C and 3D). Binding was saturable, and nonlinear fitting

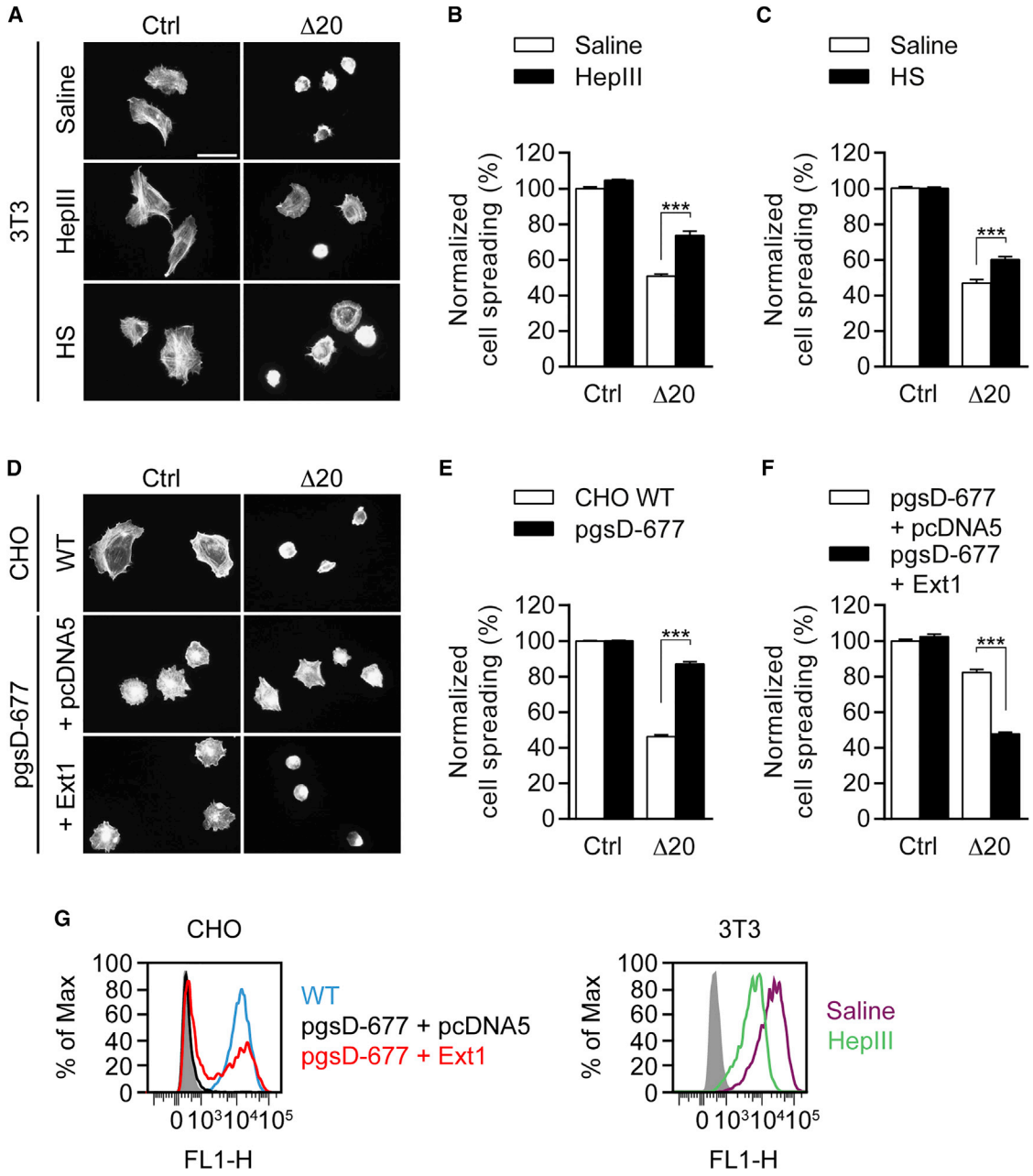

Figure 1. Cell-Surface HSPGs Mediate Nogo-A-Δ20 Inhibition of Cell Spreading

(A) Representative pictures of 3T3 fibroblasts treated with 2.5 U/mL HepIII, 0.1 mg/mL HS, or vehicle (saline) and plated on a control (ctrl) or Nogo-A-Δ20 (Δ20) substrate. Cells were stained with Phalloidin-Alexa488.

(B and C) Cell-spreading quantification of A. HepIII (B) or HS (C) treatment partially reversed Nogo-A-Δ20-mediated cell-spreading inhibition.

(D) Representative pictures of CHO WT, CHO pgsD-677, or CHO pgsD-677 expressing *Ext1* cDNA and plated on a control or Nogo-A-Δ20 substrate.

(E and F) Cell-spreading quantification of the groups shown in (D) and of mock-transfected CHO pgsD-677 cells (pgsD-677 + pCDNA5). (E) The rounding response to Nogo-A-Δ20 is highly impaired in CHO pgsD-677 mutants. (F) Expression of EXT1 in CHO pgsD-677 cells fully restored Nogo-A-Δ20 inhibition.

(G) Flow cytometry detection of cell-surface HSPGs in 3T3 cells or CHO WT and pgsD-677 cells using the 10E4 antibody. HepIII treatment of 3T3 cells reduces HSPG levels. EXT1 expression restores HSPG levels in CHO pgsD-677 cells. WT designates CHO cells. Filled gray curves indicate unstained controls. The fluorescence intensity is displayed on the x axis (256 bins) and the normalized number of cells per bin on the y axis.

Data shown are means ± SEM (n = 8–12 coverslips). (B, C, E, and F) One-way ANOVA with Tuckey's post hoc test (***$p < 0.001$). Scale bars, 45 μm. See also Figure S1.

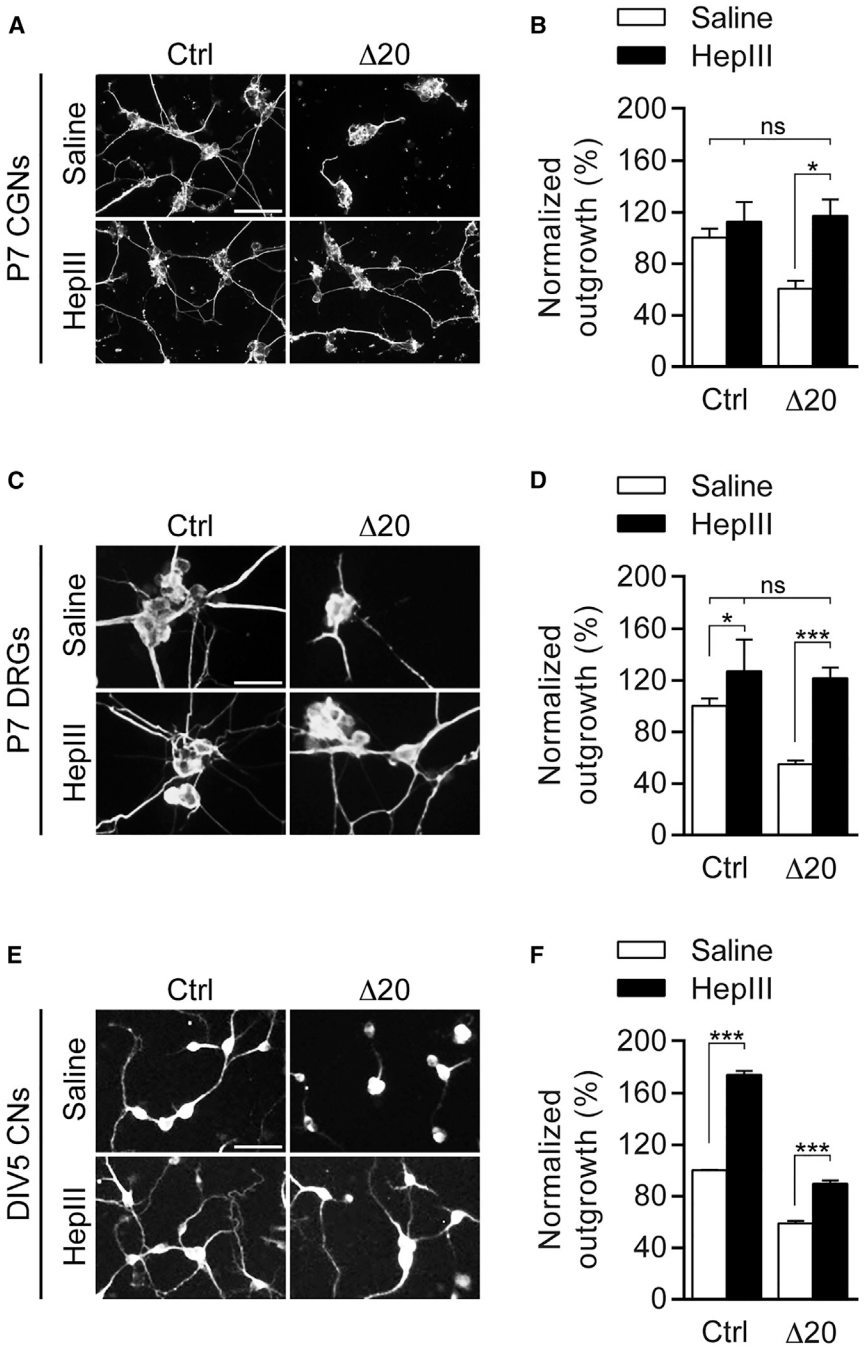

Figure 2. Cell-Surface HSPGs Mediate Nogo-A-Δ20 Inhibition of Neurite Outgrowth

(A) Representative pictures of mouse P7 cerebellar granule neurons (CGNs) treated with 500 mU/mL HepIII or vehicle (saline) and plated on a control (ctrl) or Nogo-A-Δ20 (Δ20) substrate. Neurons were stained with βIII-Tubulin.

(B) Total neurite length per cell quantification of (A). HepIII treatment fully reversed Nogo-A-Δ20-mediated inhibition of neurite outgrowth.

(C) Representative pictures of mouse P7 dorsal root ganglia (DRG) neurons treated with 1 U/ml HepIII or vehicle (saline) and plated on a control or Nogo-A-Δ20 (Δ20) substrate. Neurons were stained with βIII-Tubulin.

(D) Total neurite length per cell quantification of (C).

(E) Representative pictures of DIV5 rat E19 cortical neurons (CNs) treated with 1 U/mL HepIII or vehicle (saline) at DIV4 and replated on a control (ctrl) or Nogo-A-Δ20 (Δ20) substrate for 24 hr. Neurons were stained with Map1b.

(F) Total neurite length per cell quantification of (E). DIV, days *in vitro*.

Data shown are means ± SEM (n = 3–9 coverslips). (B, D, and F) One-way ANOVA with Tuckey's post hoc test (*$p < 0.05$, ***$p < 0.001$; ns: not significant). Scale bars, 45 μm.

revealed that Nogo-A-Δ20 binds to heparin and HS-GAGs with a dissociation constant (K_d) of ~234 nM and ~562 nM, respectively (Figures 3C and 3D).

To assess the ability of Nogo-A-Δ20 to bind HS under physiological conditions, cell-surface binding assays were performed in CHO WT and pgsD-677 cells. Cells were incubated with HA-tagged Nogo-A-Δ20 for 1 hr at 4°C, washed, and immunostained for the HA tag (Figure 3E). Nogo-A-Δ20 binding was assessed by measuring the number of Nogo-A-Δ20 puncta per cell-surface area calculated upon 3D reconstruction of the cells. High numbers of Nogo-A-Δ20 puncta per WT CHO cell were found, whereas no binding of Nogo-A-Δ20 was detected in CHO pgs-D677 cells (Figure 3F). Similar results were obtained in 3T3 cells after HepIII treatment (Figure 3G), showing that Nogo-A-Δ20 binds HSPGs in a physiological setting.

Nogo-A-Δ20 Acts via HSPGs Independently of S1PR2

Cell-surface HSPGs can act as co-receptors by promoting the binding of a ligand to its obligate receptor and thereby altering its activation (Bernfield et al., 1999; Sarrazin et al., 2011). Given the prior identification of the G-protein-coupled receptor (GPCR), S1PR2, as a functional receptor for Nogo-A-Δ20 (Kempf et al., 2014), HSPGs may enhance or allow the formation of a Nogo-A-Δ20/S1PR2 complex. Alternatively, HSPGs may transduce Nogo-A-Δ20 signals independently of S1PR2. In the latter case, we reasoned that HepIII treatment of S1PR2-deficient cells should show a disinhibition effect; in the former case, no effect of HepIII should be observed given the requirement of S1PR2 as obligate receptor. To test this, $S1PR2^{-/-}$ mouse embryonic fibroblasts (MEFs) (Kempf et al., 2014) were treated with HepIII or saline and plated on Nogo-A-Δ20. Strikingly, treatment of $S1PR2^{-/-}$ MEFs with HepIII significantly further increased cell spreading on Nogo-A-Δ20 when compared with HepIII-treated WT MEFs or $S1PR2^{-/-}$ MEFs alone (Figures 4A and S3A). This suggests that Nogo-A-Δ20 can act via HSPGs independently of S1PR2.

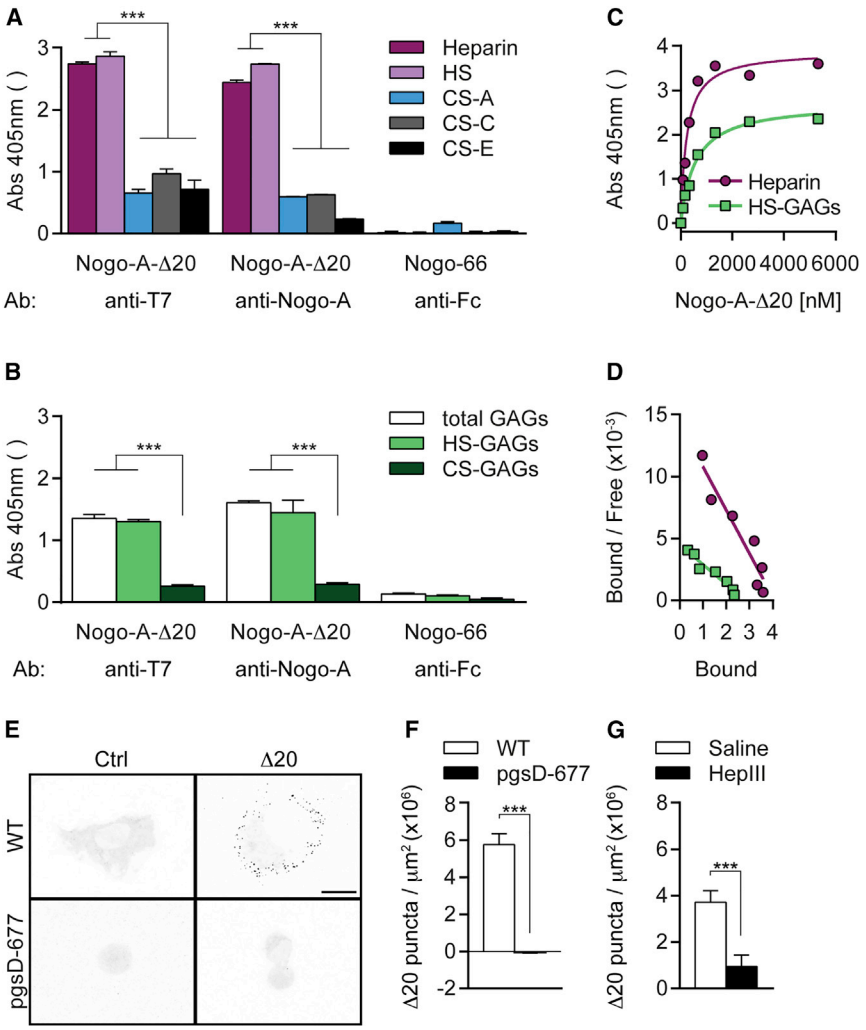

Figure 3. Nogo-A-Δ20, but Not Nogo-66, Binds Heparin and HS

(A–D) Biotinylated heparin, HS, CS, or brain-derived GAGs were coated onto streptavidin-coated wells and analyzed for Nogo-A-Δ20 or Nogo-66 binding by an ELISA assay. Average values for the BSA negative control were subtracted from the respective readings. Nogo-A-Δ20-T7 binding was detected using an anti-T7 or anti-Nogo-A (11c7) antibody and Nogo-66-Fc binding using an anti-Fc antibody. (A) Binding analysis of Nogo-A-Δ20 and Nogo-66 to heparin, HS, CS-A, CS-C, or CS-E. (B) Binding analysis of Nogo-A-Δ20 and Nogo-66 to brain-derived GAGs treated with heparinase (CS-GAGs) or chondroitinase ABC (HS-GAGs). Total GAGs refer to the untreated GAG fraction. (C) Saturation curve of Nogo-A-Δ20 to heparin ($K_d \sim 234$ nM) and brain-derived HS-GAGs ($K_d \sim 562$ nM). Detection was performed using the anti-T7 antibody. (D) Scatchard plot of (C).

(E) Representative images of cell-surface binding of Nogo-A-Δ20 to CHO WT and HSPG-deficient CHO pgsD-677 cells. Cells were incubated with 1 μM HA-tagged Nogo-A-Δ20 for 30 min on ice and stained using the anti-HA antibody.

(F and G) Quantification of cell-surface binding by assessing the number of bound HA-tagged Nogo-A-Δ20 spots in CHO WT and pgsD-677 cells (F) or in HepIII versus saline-treated 3T3 cells (G). Average values for the control were subtracted from the respective measurements.

Data shown are means ± SEM. (A–D) n = 3 experiments; (F) n = 10 cells; (G) n = 30–34 cells. (A and B) One-way ANOVA with Tuckey's post hoc test; (F and G) Mann-Whitney test (***$p < 0.001$). Scale bar, 15 μm. See also Figure S2.

In CHO-K1 WT cells, the levels of endogenous S1PRs' mRNAs were shown to be below detection limit, and these cells were unresponsive to the S1PR family ligand S1P in a variety of *in vitro* assays (e.g., Gonda et al., 1999; Okamoto et al., 1998). Based on these observations, CHO-K1 WT cells are considered as devoid of S1PR expression. To validate this under our experimental conditions, CHO WT cells were treated with the pharmacological S1PR2 antagonist, JTE-013, and plated onto Nogo-A-Δ20 and control substrates (Figures 4B and S3B). As expected, JTE-013 did not antagonize Nogo-A-Δ20-dependent inhibition of cell spreading (Figures 4B and S3B), suggesting that Nogo-A-Δ20 can exert inhibitory effects via HSPGs in S1PR2-deficient cellular systems. Also, JTE-013 did not antagonize Nogo-A-Δ20-dependent inhibition of cell spreading in mutant pgsD-677 cells (Figures 4B and S3B).

Nogo-A-Δ20 has been repeatedly shown to activate the RhoA/ROCK pathway and thereby to inhibit cell spreading and neurite outgrowth (Kempf et al., 2014; Niederost et al., 2002). To test whether HSPGs can also mediate Nogo-A-Δ20-induced downstream signaling, RhoA activation was measured in CHO WT and pgsD-677 cells. In CHO WT cells, a ~250% increase in RhoA activation was observed 20 min after application of Nogo-A-Δ20, whereas no change was observed in pgsD-677 cells (Figures 4C and 4D). The inactive Nogo-A fragment Nogo-A-Δ21 was used as control protein. Further, no change in RhoA activation was observed in the presence of JTE-013 (Figure S4), suggesting the presence of an S1PR2-independent, HSPG-dependent Nogo-A-Δ20 signal transduction pathway.

To determine whether Nogo-A-Δ20 inhibition in CHO WT cells could be overcome by blocking RhoA or the downstream Rho-associated kinase (ROCK), CHO WT cell were treated with the RhoA inhibitor, C3 transferase, or with the ROCK inhibitor, Y-27632, and plated onto Nogo-A-Δ20. In line with the RhoA activation results, blockade of RhoA or ROCK showed a full rescue of Nogo-A-Δ20 inhibition (Figures 4E and 4F).

Finally, in order to determine the effect of simultaneous blockade of HSPGs and S1PR2 in cells co-expressing HSPGs and S1PR2, 3T3 cells were treated with HepIII and/or JTE-013 and assessed in a cell-spreading assay. Strikingly, blockade of HSPGs and S1PR2 showed an additive effect in reducing Nogo-A-Δ20-induced inhibition of cell spreading

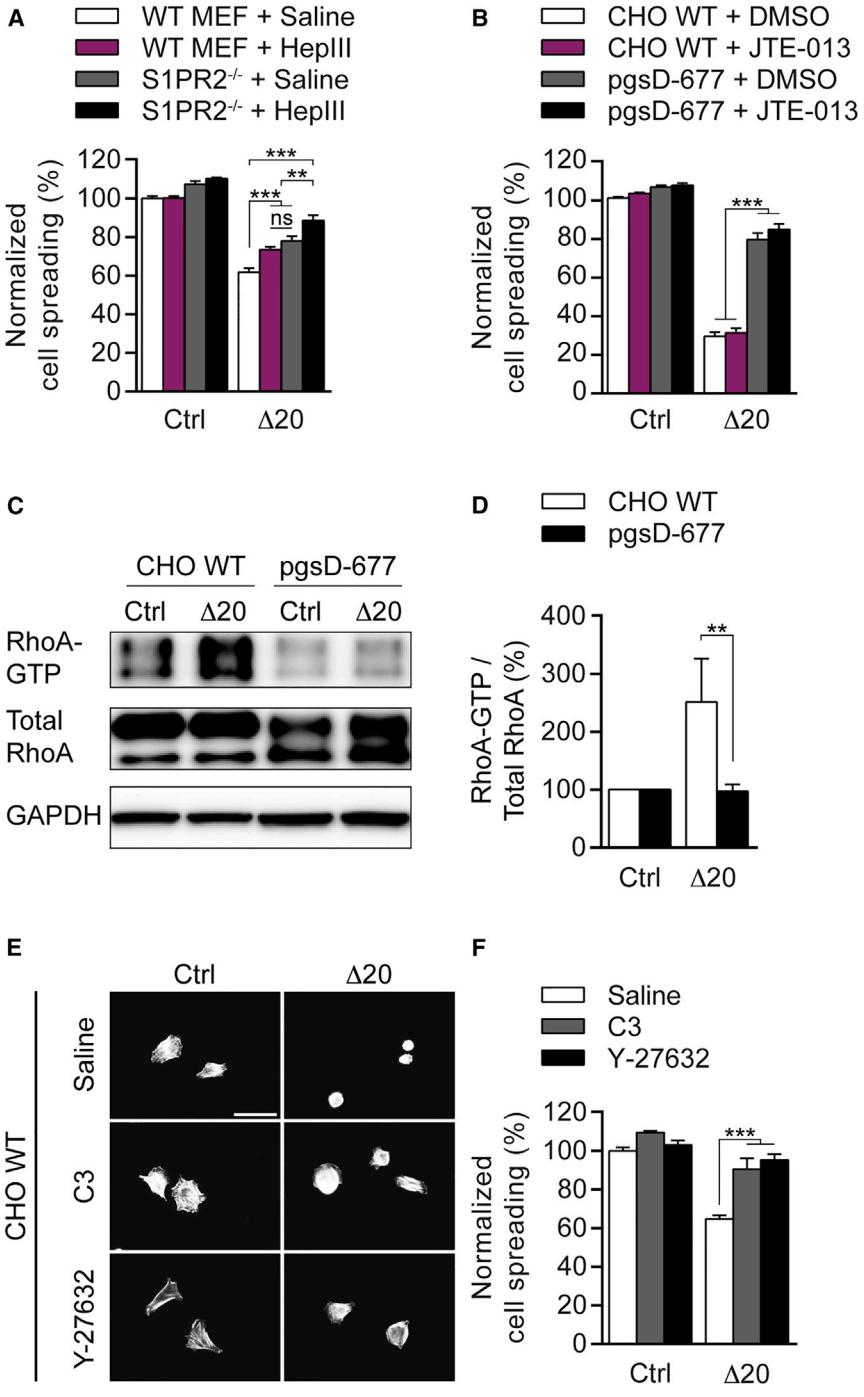

Figure 4. HSPGs Mediate Nogo-A-Δ20 Signaling Independently of S1PR2

(A) Cell-spreading quantification of CHO WT and CHO pgsD-677 cells treated with 1 μM JTE-013 or vehicle (DMSO) and plated on a control (ctrl) or Nogo-A-Δ20 (Δ20) substrate. Representative pictures are shown in Figure S3A.

(B) Cell-spreading quantification of WT and S1PR2$^{-/-}$ MEFs treated with 2.5 U/mL HepIII or vehicle (saline) and plated on a control (ctrl) or Nogo-A-Δ20 (Δ20) substrate. Representative pictures are shown in Figure S3B.

(C) RhoA activation was assessed in CHO WT and pgsD-677 cells 20 min post-incubation with 1 μM Nogo-A-Δ20 by western blotting.

(D) Quantification of RhoA-GTP/Total RhoA levels shown in (C). Nogo-A-Δ20 does not activate RhoA in pgsD-677 cells.

(E) Representative pictures of CHO WT cells treated with the RhoA inhibitor C3 transferase (0.1 mg/mL), the ROCK blocker Y-27632 (5 μM), or vehicle (saline).

(F) Cell-spreading quantification of (E).

Data shown are means ± SEM. (B and F) n = 6–16 coverslips; (D) n = 3 experiments. (A, B, D, and F) One-way ANOVA with Tuckey's post hoc test (**p < 0.01; ***p < 0.001). Scale bars, 45 μm. See also Figures S3 and S4.

opposed to syndecans, glypicans are attached by a glycosylphosphatidylinositol anchor to the membrane and do not exert cytoplasmic signaling roles (Bernfield et al., 1999). The syndecan family consists of four members: syndecan-1 to syndecan-4 (Sdc1–Sdc4) (Bernfield et al., 1999), of which syndecan-4 is the most highly expressed in 3T3 cells (Figure 5A). Interestingly, syndecan-4 has been shown to activate RhoA to promote focal adhesion maturation and stress fiber assembly following engagement with fibronectin (Brooks et al., 2012; Dovas et al., 2006).

To test the contribution of syndecan-4 to Nogo-A-Δ20-induced inhibition of cell spreading and RhoA activation, syndecan-4 was knocked down using lentivirus-delivered control and syndecan-4 shRNA (Figure S5A). Strikingly, knockdown of syndecan-4 fully prevented Nogo-A-Δ20 inhibition of cell spreading (Figures 5B and 5C). To test if Nogo-A-Δ20 activates RhoA via syndecan-4, RhoA activation assays were performed in control versus syndecan-4 shRNA cells. The inactive Nogo-A fragment, Nogo-A-Δ21, was used as control protein. No RhoA activation was observed upon syndecan-4 knockdown (Figure 5G). Together, these results suggest that Nogo-A-Δ20 inhibits cell spreading by activating RhoA via syndecan-4 in fibroblasts.

To investigate whether syndecans are also important in Nogo-A-Δ20-induced inhibition of neurite outgrowth, we first assessed

(Figures S3C and S3D). Hence, in cells co-expressing both receptors, Nogo-A-Δ20 can exert inhibitory effects via both S1PR2 as well as HSPGs. However, as shown by using S1PR2-deficient cells, HSPGs are themselves sufficient to mediate Nogo-A-Δ20 inhibition and RhoA activation.

Syndecans Mediate Nogo-A-Δ20 Inhibition of Cell Spreading and Neurite Outgrowth

Membrane-bound cell-surface HSPGs consist of two main families: syndecans and glypicans (Bernfield et al., 1999). As

their expression in DIV4 E19 rat cortical neurons and found syndecan-3 to be the most highly expressed (Figure 5D). Remarkably, siRNA-mediated knockdown of syndecan-3 fully prevented outgrowth inhibition on the Nogo-A-Δ20 substrate (Figures 5E, 5F, and S5B).

Further, to test whether syndecan-3 and syndecan-4 directly interact with Nogo-A-Δ20, microscale thermophoresis binding experiments were performed using recombinant syndecan-3 and syndecan-4 proteins. We found that Nogo-A-Δ20 binds to syndecan-3 and syndecan-4 in a similar affinity range as it binds to brain-derived HS-GAGs with a K_d of ~865.7 nM and ~522.1 nM, respectively (Figure 5H). Taken together, these data show that Nogo-A-Δ20 binds to and exerts inhibitory effects via syndecan-3 or -4 in a cell-type-specific manner.

Nogo-A-Δ20 Promotes Neuroblast Migration via HSPGs

Nogo-A-Δ20 was shown to promote the tangential migration of neuroblasts from the subventricular zone (SVZ) to the olfactory bulb along the rostral migratory stream (RMS) through activation of the Rho/ROCK pathway (Rolando et al., 2012). Yet, no molecular basis for this observation was found, and we sought to determine the physiological relevance of the Nogo-A-Δ20/HSPG interaction in this process.

To investigate the contribution of HSPGs to SVZ-derived neuroblast migration, postnatal explants of the SVZ and RMS were used as an *ex vivo* model (Wichterle et al., 1997) and treated with HepIII and/or the Nogo-A-Δ20 function-blocking antibody 11c7. In this assay, neuroblasts move out of the explant core by chain migration (i.e., associated with each other) as occurs in the RMS *in vivo* (Wichterle et al., 1997). As previously shown, Nogo-A neutralization by 11c7 induced a significant reduction of the migration area (Figures 6A and 6B). HepIII treatment induced a similar reduction of the migration (Figures 6A and 6B). To examine whether HSPGs and Nogo-A-Δ20 operate through the same pathway, we co-administered HepIII and 11c7. Co-application of HepIII and 11c7 led to a reduction in migration area similar to that obtained upon treatment of HepIII or 11c7 alone (Figures 6A and 6B), suggesting that Nogo-A-Δ20 operates through HSPGs in this system.

Previous data suggested that Nogo-A sustains neuroblast migration by providing anti-adhesive signals (Rolando et al., 2012). To investigate whether HSPGs participate in Nogo-A-Δ20-mediated repulsive effects, we asked whether HepIII treatment affected neuroblast adhesion on control versus Nogo-A-Δ20-coated substrates in the presence or absence of 11c7. HepIII treatment significantly increased cell adhesion on Nogo-A-Δ20 to a similar extent to 11c7 (Figure 6C). No additive or synergistic effects were observed (Figure 6C), suggesting that Nogo-A-Δ20 and HSPGs share a common pathway in *ex vivo* cultures.

Finally, to test the role of the previously identified Nogo-A-Δ20 receptor S1PR2 in neuroblast migration, explants were treated with the S1PR2 blocker, JTE-013, or DMSO (vehicle control). No significant effect on the migration area was observed using different concentrations of JTE-013 (Figures 6D and 6E). Similarly, JTE-013 treatment had no effect on neuroblast adhesion (Figure 6F). Taken together, these data show that Nogo-A-Δ20 inhibits adhesion and increases migration by providing anti-adhesive signals through HSPGs but not S1PR2.

DISCUSSION

Cell-to-cell signaling by ligand receptor interactions as well as interactions with ECM constituents play key roles during developmental processes such as neuronal migration and axon growth. In this study, we identify a biochemical interaction between the membrane protein Nogo-A and HSPGs and demonstrate its functional significance in cell spreading, neurite outgrowth, adhesion, and neuroblast chain migration.

Cell-surface HSPGs are traditionally viewed as co-receptors that promote the binding of a ligand to its obligate receptor through their large glycosaminoglycan chains (Bernfield et al., 1999; Sarrazin et al., 2011) but do not act as signal-transducing receptors themselves. In the case of FGF and many other morphogens, HS is essential for the ligand/receptor complex to form and to alter its activation (Sarrazin et al., 2011). Surprisingly, our data suggest that this is not the case for Nogo-A-Δ20 and its S1PR2 receptor (Kempf et al., 2014): Nogo-A-Δ20 can activate RhoA in S1PR-negative CHO cells and inhibits cell spreading in S1PR2$^{-/-}$ MEFs. Hence, our results strongly suggest that Nogo-A-Δ20 can signal through S1PR-independent mechanisms. However, when HSPGs and S1PR2 are co-expressed, both pathways can act in parallel, as shown for fibroblasts, or one pathway can gain control of the signaling output, as demonstrated for neuroblasts. Collectively, our experiments reveal that more than one receptor for the active Nogo-A-Δ20 region exists and that Nogo-A-Δ20-induced inhibitory effects are regulated in a cell-type-specific manner.

Based on our findings showing the involvement of syndecan-3 and syndecan-4, we may hypothesize that the cytoplasmic tail of syndecans is important for Nogo-A-Δ20-induced signal transduction upon extracellular binding to the HS chains. A few studies have shown that transmembrane syndecans can act as signaling receptors through their cytoplasmic domains. During cell migration, engagement of syndecan-4 by fibronectin was shown to result in the activation of protein kinase C α (PKCα) upstream of RhoA activation (Bass et al., 2007, 2008; Brooks et al., 2012; Dovas et al., 2006). Even though it is unclear how syndecan-4 signals to RhoA via PKCα, PKCα was shown to activate RhoA via phosphorylation of the Rho guanine exchange factor (RhoGEF), p115, in a different system (Peng et al., 2011). It will be interesting to investigate if Nogo-A-Δ20 operates via similar mechanisms. In the case of syndecan-3, binding of the heparin-binding growth-associated molecule (HB-GAM) was shown to result in phosphorylation of the Src kinases, c-Src and c-Fyn, and of cortactin, which promotes polymerization and rearrangement of the actin cytoskeleton resulting in neurite outgrowth (Kinnunen et al., 1998). A similar mechanism was proposed for glial cell line-derived neurotrophic factor (GDNF) family ligands and syndecan-3 (Bespalov et al., 2011). However, no link between syndecan-3 and RhoA activation has been reported so far and future studies will address this point.

Syndecan-3 is the major HSPG found in neurons of the developing brain and shows abundant expression in major axonal tracts and migratory routes, e.g., in the RMS (Hienola

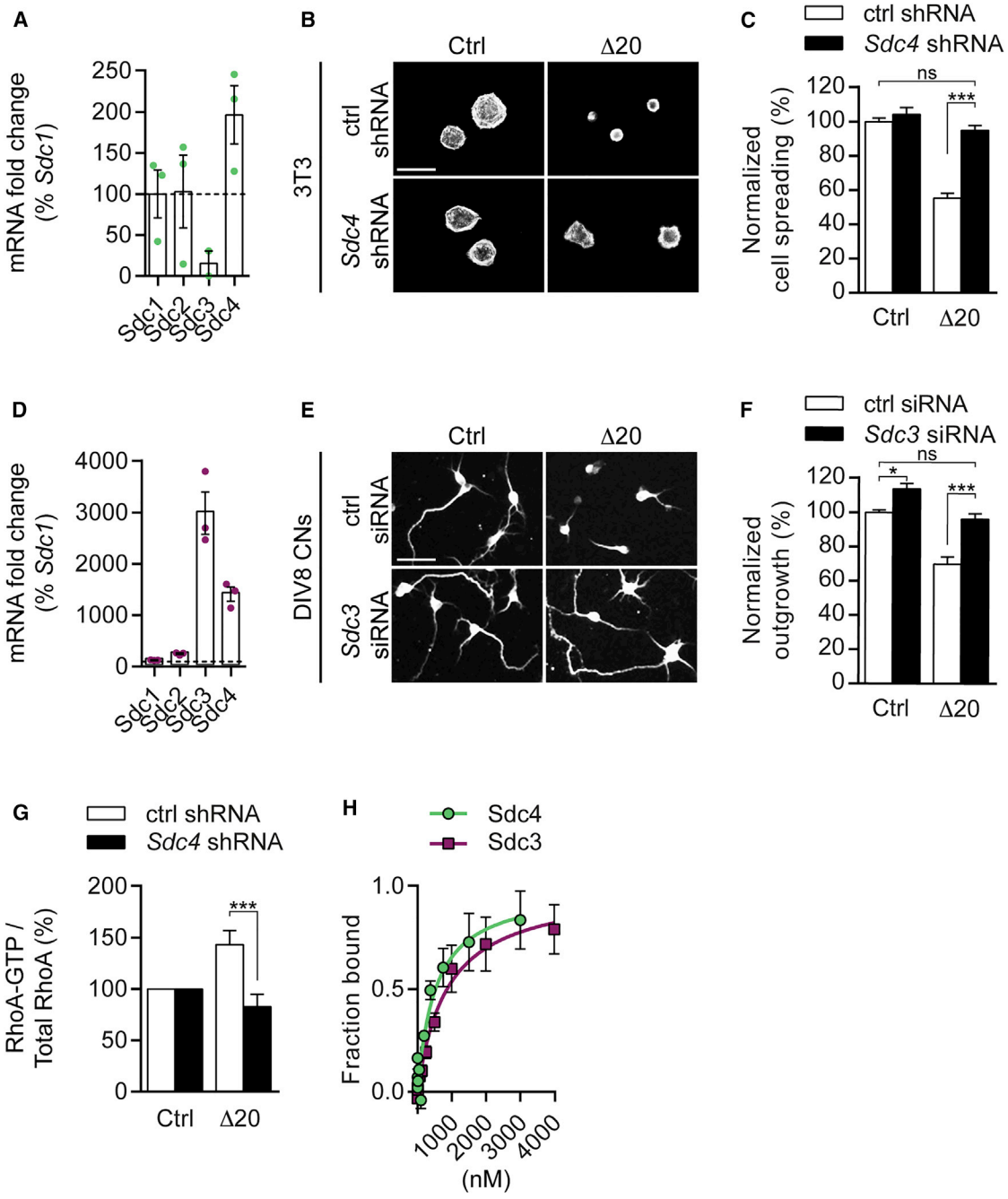

Figure 5. Syndecans Mediate Nogo-A-Δ20 Inhibition of Cell Spreading and Neurite Outgrowth

(A) qRT-PCR expression analysis of syndecans (Sdcs) in 3T3 cells. mRNA fold changes are normalized to the expression values of Sdc1 obtained in the first experiment.

(B) Representative pictures of 3T3 cells stably expressing *Sdc4* or ctrl shRNA and replated on a control (ctrl) or Nogo-A-Δ20 (Δ20) substrate for 1 hr. Cells were stained with Phalloidin-Alexa488.

(C) Cell-spreading quantification of (B).

(D) qRT-PCR expression analysis of Sdcs in DIV4 rat E19 cortical neurons. mRNA fold changes are normalized to the expression values of Sdc1 obtained in the first experiment.

(E) Representative pictures of DIV8 rat cortical neurons treated at DIV4 with control (ctrl) or *Sdc3* siRNA for 72 hr and replated on a ctrl or Nogo-A-Δ20 (Δ20) substrate for 24 hr. Cells were stained with MAP1b.

(F) Neurite length quantification of (E).

(G) RhoA activation was assessed in 3T3 cells expressing *Sdc4* or ctrl shRNA 20 min post-incubation with 1 μM Nogo-A-Δ20 using a commercially available ELISA kit. Quantification of RhoA-GTP/total RhoA levels is shown.

(legend continued on next page)

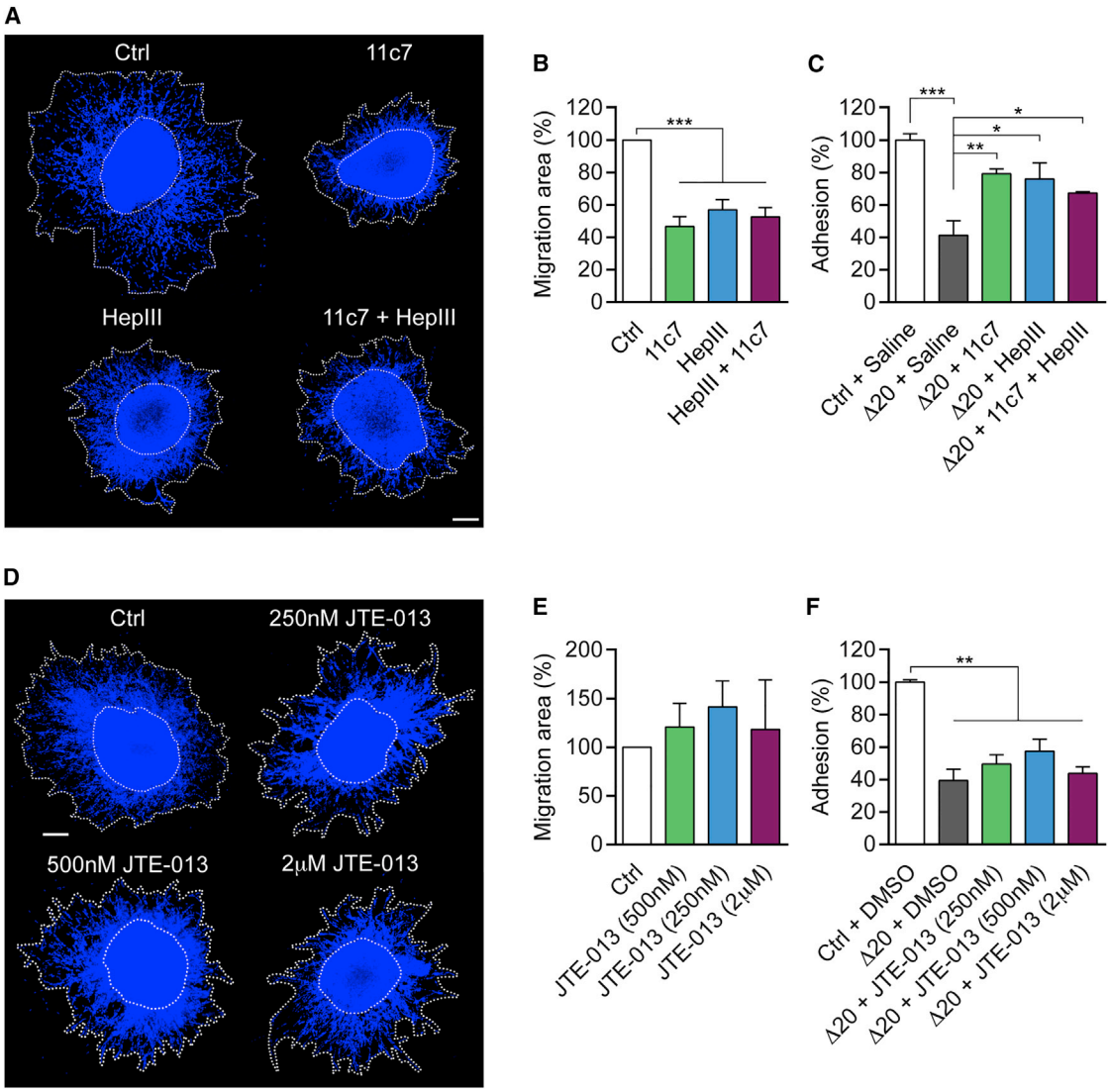

Figure 6. Nogo-A-Δ20 Regulates Neuroblast Adhesion and Migration via HSPGs

(A) Representative pictures of neuroblast explants (SVZ and RMS) showing the decrease in migration area of HepIII (500 mU/mL), 11c7 (1 μg/μL), and HepIII+11c7-treated explants versus controls.

(B) Quantification of the migration area. Controls are set to 100% for each experiment.

(C) Adhesion of SVZ-dissociated neuroblasts on a Nogo-A-Δ20 substrate after treatment with 11c7 and/or HepIII. No synergistic activity is detected by co-treatment of neuroblasts with 11c7 and HepIII in (B) and (C).

(D) Representative pictures of neuroblast explants (SVZ and RMS) treated with different concentrations of JTE-013 or vehicle (DMSO).

(E) Quantification of the migration in the presence of JTE-013 versus DMSO. Controls are set to 100% for each experiment.

(F) Adhesion of SVZ-dissociated neuroblasts on a Nogo-A-Δ20 substrate after treatment with JTE-013 or DMSO.

No effect is observed upon treatment with JTE-013 in (E) and (F). Data shown are means ± SEM. (B) n = 4–5 experiments; (C) n = 3 coverslips; (E) n = 4–5 experiments; (F) n = 3–4 coverslips. (B, C, and F) One-way ANOVA with Bonferroni's post hoc test (*$p < 0.05$, **$p < 0.01$, ***$p < 0.001$). Scale bars, (A and D) 100 μm.

et al., 2006; Nolo et al., 1995; Rauvala et al., 2000). In the adult brain, syndecan-3 is strongly expressed in the hippocampus, cerebellum, and cortex, and in several axonal tracts (Hsueh and Sheng, 1999). Our results show that the anti-adhesive effect of Nogo-A-Δ20 is accompanied by an HS-dependent increase in neuroblast chain migration. Notably, syndecan-$3^{-/-}$ mice phenocopy the defects in radial and tangential neuronal migration observed in Nogo-$A^{-/-}$ mice (Hienola

(H) Microscale binding analysis of Nogo-A-Δ20 to recombinant mouse Sdc4 ($K_d \sim 522.1$ nM) or Sdc3 ($K_d \sim 865.7$ nM). Single dots indicate biological replicates in (A) and (D).

Data shown are means ± SEM (A and D) n = 3 experiments; (G) n = 6 experiments; (C and F) n = 8–16 coverslips. (C, F, and G) One-way ANOVA with Tuckey's post hoc test (*$p < 0.05$, ***$p < 0.001$; ns: not significant). Scale bars, 45 μm. See also Figure S5.

et al., 2006; Mathis et al., 2010; Mingorance-Le Meur et al., 2007; Rolando et al., 2012). Syndecan-3$^{-/-}$ mice also display a synaptic plasticity phenotype similar to that observed in Nogo-A$^{-/-}$ mice, increasing CA1 long-term potentiation (LTP) while baseline transmission and short-term plasticity are not affected (Kaksonen et al., 2002). Given the recent implication of HSPGs in synapse formation and plasticity (Allen et al., 2012; de Wit et al., 2013; Siddiqui et al., 2013), it will be interesting to determine if Nogo-A also mediates its effects on synapse formation and plasticity via HSPGs (Mironova and Giger, 2013). Overall, the localization of syndecan proteins and their physiological impact in the developing and adult brain are consistent with a functional interaction between Nogo-A and HSPGs *in vivo*.

In conclusion, our study shows that Nogo-A-Δ20 regulates adhesion, cell spreading, outgrowth, and migration of various cell lines, neurons, and neuroblasts by interacting with transmembrane HSPGs.

STAR★METHODS

Detailed methods are provided in the online version of this paper and include the following:

- KEY RESOURCE TABLE
- CONTACT FOR REAGENT AND RESOURCE SHARING
- EXPERIMENTAL MODEL AND SUBJECT DETAILS
  - Primary Neuronal Cultures and Explants
  - Cell Lines
- METHOD DETAIL
  - Constructs and Protein Expression
  - Brain-Derived Glycosaminoglycans (GAGs)
  - Spinal Cord Protein Extracts
  - MEF Isolation
  - Immunocytochemistry
  - Flow Cytometry
  - RhoA Activation Assays
  - Generation of Stable Cell Lines
  - Cell Spreading and Neurite Outgrowth Assays
  - Quantitative Real-Time PCR (qRT-PCR)
  - ELISA
  - Explant Assay
  - Adhesion Assay
  - Microscale Thermophoresis
- QUANTIFICATION AND STATISTICAL ANALYSIS

SUPPLEMENTAL INFORMATION

Supplemental Information includes five figures and can be found with this article online at http://dx.doi.org/10.1016/j.devcel.2017.08.014.

AUTHOR CONTRIBUTIONS

A.K. and M.E.S conceived and designed the research. A.K. performed cell-spreading and neurite outgrowth experiments, cell-surface binding experiments, RhoA activation assays, qRT-PCR experiments, and data analysis with the help of A.M.K., Z.R., B.T., R.F., and O.P. Microscale thermophoresis experiments were performed by Andre and Antonio Schmandke and assisted by A.K. Flow cytometry experiments were performed by Z.R. and assisted by A.K. ELISA experiments and data analysis were performed by J.C.F.K. and J.W.F. Neuroblast migration, SVZ cell adhesion experiments, and data analysis were performed by E.B., V.G., and A.B. The paper was written by A.K. and M.E.S., and all authors made comments.

ACKNOWLEDGMENTS

We thank H. Rauvala for helpful discussions and J. Esko for providing *Ext1* cDNA. We thank Ruth Brain and Anne Engmann for proofreading the manuscript. This work was supported by the Swiss National Science Foundation (grants 3100A0-122527/1 and 310030B- 138676/1), the ERC advanced grant 294115 "Nogorise" and the National Centre for Competence in Research "Neural Plasticity and Repair" of the Swiss National Science Foundation. M.E.S is a founder and board member of the University of Zurich spin-off company NovaGo Therapeutics Inc., seeking to develop Nogo-A-neutralizing therapies.

Received: July 12, 2016
Revised: July 4, 2017
Accepted: August 21, 2017
Published: September 21, 2017

REFERENCES

Allen, N.J., Bennett, M.L., Foo, L.C., Wang, G.X., Chakraborty, C., Smith, S.J., and Barres, B.A. (2012). Astrocyte glypicans 4 and 6 promote formation of excitatory synapses via GluA1 AMPA receptors. Nature *486*, 410–414.

Bass, M.D., Roach, K.A., Morgan, M.R., Mostafavi-Pour, Z., Schoen, T., Muramatsu, T., Mayer, U., Ballestrem, C., Spatz, J.P., and Humphries, M.J. (2007). Syndecan-4-dependent Rac1 regulation determines directional migration in response to the extracellular matrix. J. Cell Biol. *177*, 527–538.

Bass, M.D., Morgan, M.R., Roach, K.A., Settleman, J., Goryachev, A.B., and Humphries, M.J. (2008). p190RhoGAP is the convergence point of adhesion signals from alpha 5 beta 1 integrin and syndecan-4. J. Cell Biol. *181*, 1013–1026.

Bernfield, M., Gotte, M., Park, P.W., Reizes, O., Fitzgerald, M.L., Lincecum, J., and Zako, M. (1999). Functions of cell surface heparan sulfate proteoglycans. Annu. Rev. Biochem. *68*, 729–777.

Bespalov, M.M., Sidorova, Y.A., Tumova, S., Ahonen-Bishopp, A., Magalhaes, A.C., Kulesskiy, E., Paveliev, M., Rivera, C., Rauvala, H., and Saarma, M. (2011). Heparan sulfate proteoglycan syndecan-3 is a novel receptor for GDNF, neurturin, and artemin. J. Cell Biol. *192*, 153–169.

Brooks, R., Williamson, R., and Bass, M. (2012). Syndecan-4 independently regulates multiple small GTPases to promote fibroblast migration during wound healing. Small GTPases *3*, 73–79.

de Wit, J., O'Sullivan, M.L., Savas, J.N., Condomitti, G., Caccese, M.C., Vennekens, K.M., Yates, J.R., 3rd, and Ghosh, A. (2013). Unbiased discovery of glypican as a receptor for LRRTM4 in regulating excitatory synapse development. Neuron *79*, 696–711.

Deepa, S.S., Carulli, D., Galtrey, C., Rhodes, K., Fukuda, J., Mikami, T., Sugahara, K., and Fawcett, J.W. (2006). Composition of perineuronal net extracellular matrix in rat brain: a different disaccharide composition for the net-associated proteoglycans. J. Biol. Chem. *281*, 17789–17800.

Dovas, A., Yoneda, A., and Couchman, J.R. (2006). PKCbeta-dependent activation of RhoA by syndecan-4 during focal adhesion formation. J. Cell Sci. *119*, 2837–2846.

Gonda, K., Okamoto, H., Takuwa, N., Yatomi, Y., Okazaki, H., Sakurai, T., Kimura, S., Sillard, R., Harii, K., and Takuwa, Y. (1999). The novel sphingosine 1-phosphate receptor AGR16 is coupled via pertussis toxin-sensitive and -insensitive G-proteins to multiple signalling pathways. Biochem. J. *337* (Pt 1), 67–75.

Hienola, A., Tumova, S., Kulesskiy, E., and Rauvala, H. (2006). N-syndecan deficiency impairs neural migration in brain. J. Cell Biol. *174*, 569–580.

Hovingh, P., and Linker, A. (1970). The enzymatic degradation of heparin and heparitin sulfate. 3. Purification of a heparitinase and a heparinase from flavobacteria. J. Biol. Chem. *245*, 6170–6175.

Hsueh, Y.P., and Sheng, M. (1999). Regulated expression and subcellular localization of syndecan heparan sulfate proteoglycans and the syndecan-binding protein CASK/LIN-2 during rat brain development. J. Neurosci. *19*, 7415–7425.

Hu, H. (2001). Cell-surface heparan sulfate is involved in the repulsive guidance activities of Slit2 protein. Nat. Neurosci. *4*, 695–701.

Inatani, M., Irie, F., Plump, A.S., Tessier-Lavigne, M., and Yamaguchi, Y. (2003). Mammalian brain morphogenesis and midline axon guidance require heparan sulfate. Science *302*, 1044–1046.

Irie, F., Okuno, M., Matsumoto, K., Pasquale, E.B., and Yamaguchi, Y. (2008). Heparan sulfate regulates ephrin-A3/EphA receptor signaling. Proc. Natl. Acad. Sci. USA *105*, 12307–12312.

Kaksonen, M., Pavlov, I., Voikar, V., Lauri, S.E., Hienola, A., Riekki, R., Lakso, M., Taira, T., and Rauvala, H. (2002). Syndecan-3-deficient mice exhibit enhanced LTP and impaired hippocampus-dependent memory. Mol. Cell. Neurosci. *21*, 158–172.

Karlsson, T.E., Smedfors, G., Brodin, A.T., Aberg, E., Mattsson, A., Hogbeck, I., Wellfelt, K., Josephson, A., Brene, S., and Olson, L. (2016). NgR1: a tunable sensor regulating memory formation, synaptic, and dendritic plasticity. Cereb. Cortex *26*, 1804–1817.

Kempf, A., and Schwab, M.E. (2013). Nogo-A represses anatomical and synaptic plasticity in the central nervous system. Physiology (Bethesda) *28*, 151–163.

Kempf, A., Tews, B., Arzt, M.E., Weinmann, O., Obermair, F.J., Pernet, V., Zagrebelsky, M., Delekate, A., Iobbi, C., Zemmar, A., et al. (2014). The sphingolipid receptor S1PR2 is a receptor for Nogo-a repressing synaptic plasticity. PLoS Biol. *12*, e1001763.

Kinnunen, T., Kaksonen, M., Saarinen, J., Kalkkinen, N., Peng, H.B., and Rauvala, H. (1998). Cortactin-Src kinase signaling pathway is involved in N-syndecan-dependent neurite outgrowth. J. Biol. Chem. *273*, 10702–10708.

Kono, M., Mi, Y., Liu, Y., Sasaki, T., Allende, M.L., Wu, Y.P., Yamashita, T., and Proia, R.L. (2004). The sphingosine-1-phosphate receptors S1P1, S1P2, and S1P3 function coordinately during embryonic angiogenesis. J. Biol. Chem. *279*, 29367–29373.

Lidholt, K., Weinke, J.L., Kiser, C.S., Lugemwa, F.N., Bame, K.J., Cheifetz, S., Massague, J., Lindahl, U., and Esko, J.D. (1992). A single mutation affects both N-acetylglucosaminyltransferase and glucuronosyltransferase activities in a Chinese hamster ovary cell mutant defective in heparan sulfate biosynthesis. Proc. Natl. Acad. Sci. USA *89*, 2267–2271.

Mathis, C., Schroter, A., Thallmair, M., and Schwab, M.E. (2010). Nogo-a regulates neural precursor migration in the embryonic mouse cortex. Cereb. Cortex *20*, 2380–2390.

Mingorance-Le Meur, A., Zheng, B., Soriano, E., and del Rio, J.A. (2007). Involvement of the myelin-associated inhibitor Nogo-A in early cortical development and neuronal maturation. Cereb. Cortex *17*, 2375–2386.

Mironova, Y.A., and Giger, R.J. (2013). Where no synapses go: gatekeepers of circuit remodeling and synaptic strength. Trends Neurosci. *36*, 363–373.

Niederost, B., Oertle, T., Fritsche, J., McKinney, R.A., and Bandtlow, C.E. (2002). Nogo-A and myelin-associated glycoprotein mediate neurite growth inhibition by antagonistic regulation of RhoA and Rac1. J. Neurosci. *22*, 10368–10376.

Nolo, R., Kaksonen, M., Raulo, E., and Rauvala, H. (1995). Co-expression of heparin-binding growth-associated molecule (HB-GAM) and N-syndecan (syndecan-3) in developing rat brain. Neurosci. Lett. *191*, 39–42.

Oertle, T., van der Haar, M.E., Bandtlow, C.E., Robeva, A., Burfeind, P., Buss, A., Huber, A.B., Simonen, M., Schnell, L., Brosamle, C., et al. (2003). Nogo-A inhibits neurite outgrowth and cell spreading with three discrete regions. J. Neurosci. *23*, 5393–5406.

Okamoto, H., Takuwa, N., Gonda, K., Okazaki, H., Chang, K., Yatomi, Y., Shigematsu, H., and Takuwa, Y. (1998). EDG1 is a functional sphingosine-1-phosphate receptor that is linked via a Gi/o to multiple signaling pathways, including phospholipase C activation, Ca2+ mobilization, Ras-mitogen-activated protein kinase activation, and adenylate cyclase inhibition. J. Biol. Chem. *273*, 27104–27110.

Peng, J., He, F., Zhang, C., Deng, X., and Yin, F. (2011). Protein kinase C-α signals P115RhoGEF phosphorylation and RhoA activation in TNF-α-induced mouse brain microvascular endothelial cell barrier dysfunction. J. Neuroinflammation *8*, 28.

Purushothaman, A., Fukuda, J., Mizumoto, S., ten Dam, G.B., van Kuppevelt, T.H., Kitagawa, H., Mikami, T., and Sugahara, K. (2007). Functions of chondroitin sulfate/dermatan sulfate chains in brain development. Critical roles of E and iE disaccharide units recognized by a single chain antibody GD3G7. J. Biol. Chem. *282*, 19442–19452.

Rauvala, H., Huttunen, H.J., Fages, C., Kaksonen, M., Kinnunen, T., Imai, S., Raulo, E., and Kilpelainen, I. (2000). Heparin-binding proteins HB-GAM (pleiotrophin) and amphoterin in the regulation of cell motility. Matrix Biol. *19*, 377–387.

Rolando, C., Parolisi, R., Boda, E., Schwab, M.E., Rossi, F., and Buffo, A. (2012). Distinct roles of Nogo-a and Nogo receptor 1 in the homeostatic regulation of adult neural stem cell function and neuroblast migration. J. Neurosci. *32*, 17788–17799.

Sarrazin, S., Lamanna, W.C., and Esko, J.D. (2011). Heparan sulfate proteoglycans. Cold Spring Harb. Perspect. Biol. *3*, a004952.

Schwab, M.E. (2010). Functions of Nogo proteins and their receptors in the nervous system. Nat. Rev. Neurosci. *11*, 799–811.

Schwab, M.E., and Strittmatter, S.M. (2014). Nogo limits neural plasticity and recovery from injury. Curr. Opin. Neurobiol. *27*, 53–60.

Siddiqui, T.J., Tari, P.K., Connor, S.A., Zhang, P., Dobie, F.A., She, K., Kawabe, H., Wang, Y.T., Brose, N., and Craig, A.M. (2013). An LRRTM4-HSPG complex mediates excitatory synapse development on dentate gyrus granule cells. Neuron *79*, 680–695.

Strochlic, L., Dwivedy, A., van Horck, F.P., Falk, J., and Holt, C.E. (2008). A role for S1P signalling in axon guidance in the *Xenopus* visual system. Development *135*, 333–342.

Van Vactor, D., Wall, D.P., and Johnson, K.G. (2006). Heparan sulfate proteoglycans and the emergence of neuronal connectivity. Curr. Opin. Neurobiol. *16*, 40–51.

Wei, G., Bai, X., Gabb, M.M., Bame, K.J., Koshy, T.I., Spear, P.G., and Esko, J.D. (2000). Location of the glucuronosyltransferase domain in the heparan sulfate copolymerase EXT1 by analysis of Chinese hamster ovary cell mutants. J. Biol. Chem. *275*, 27733–27740.

Wichterle, H., Garcia-Verdugo, J.M., and Alvarez-Buylla, A. (1997). Direct evidence for homotypic, glia-independent neuronal migration. Neuron *18*, 779–791.

Wienken, C.J., Baaske, P., Rothbauer, U., Braun, D., and Duhr, S. (2010). Protein-binding assays in biological liquids using microscale thermophoresis. Nat. Commun. *1*, 100.

Yamaguchi, Y. (2001). Heparan sulfate proteoglycans in the nervous system: their diverse roles in neurogenesis, axon guidance, and synaptogenesis. Semin. Cell Dev. Biol. *12*, 99–106.

Zillner, K., Jerabek-Willemsen, M., Duhr, S., Braun, D., Langst, G., and Baaske, P. (2012). Microscale thermophoresis as a sensitive method to quantify protein: nucleic acid interactions in solution. Methods Mol. Biol. *815*, 241–252.

STAR★METHODS

KEY RESOURCE TABLE

REAGENT or RESOURCE	SOURCE	IDENTIFIER
Antibodies		
Goat polyclonal anti-Doublecortin	Santa Cruz	Cat#sc-8066, RRID: AB_2088494
Mouse monoclonal anti-βIII Tubulin	Sigma	Cat#T8660, RRID: AB_477590
Mouse monoclonal anti-βIII Tubulin	Promega	Cat#G7121, RRID: AB_430874
Mouse monoclonal anti-GAPDH	Abcam	Cat#ab8245, RRID: AB_2107448
Mouse monoclonal anti-Heparan Sulfate	AMSBIO	Cat#370255-1, RRID: AB_10891554
Mouse monoclonal IgMκ isotype control	BD Biosciences	Cat#557275, RRID: AB_479595
Mouse monoclonal anti-Map1b	Santa Cruz	Cat#sc-58784, RRID: AB_784553
Mouse anti-Nogo-A, 11c7	Oertle et al., 2003	Cat# Nogo-A, RRID: AB_10000213
Mouse anti-human IgG	Jackson Immunoresearch	Cat# 209-005-082, RRID: AB_2339079
Mouse monoclonal anti-T7	Millipore	Cat#69522-3, RRID: AB_11211744
Rabbit monoclonal anti-RhoA	Cell Signaling	Cat#2117S, RRID: AB_10693922
Rat monoclonal anti-HA	Roche	Cat#11867423001, RRID: AB_390918
Goat polyclonal anti-mouse IgG, Fcγ fragment-specific	Jackson Immunoresearch	Cat#115-005-071, RRID: AB_2338454
Goat polyclonal anti-mouse IgG Alexa488-conjugated	Invitrogen	Cat#A-11029, RRID: AB_138404
Goat polyclonal anti-mouse IgG HRP-conjugated	Jackson Immunoresearch	Cat#115-035-003, RRID: AB_10015289
Goat polyclonal anti-rabbit IgG HRP-conjugated	Jackson Immunoresearch	Cat#111-035-003, RRID: AB_2313567
Rat monoclonal anti-mouse IgM FITC-conjugated	BD Biosciences	Cat#553437, RRID: AB_394857
4',6-diamidino-2-phenylindole (DAPI)	Thermo Fisher Scientific	Cat#D1306, RRID: AB_2629482
Phalloidin-Alexa488	Invitrogen	Cat#A-12379, RRID: AB_2315147
Bacterial and Virus Strains		
Escherichia coli: BL21(DE3)	Sigma	Cat#CMC0014
Chemicals, Peptides, and Recombinant Proteins		
Recombinant protein: Nogo-A-Δ20-T7	Oertle et al., 2003	N/A
Recombinant protein: Nogo-A-Δ21-T7	Oertle et al., 2003	N/A
Recombinant protein: Nogo-A-20-HA	Kempf et al., 2014	N/A
Recombinant protein: Nogo-A-66-Fc	R&D Systems	Cat#3728-NG-050
Recombinant protein: Sdc3	R&D Systems	Cat#2734-SD-050
Recombinant protein: Sdc4	R&D Systems	Cat#6267-SD-050
Sodium Chondroitin Sulfate A (bovine trachea)	Sigma	Cat#C9819
Sodium Chondroitin Sulfate C (shark cartilage)	Fluka	Cat#27043
Sodium Chondroitin Sulfate E (squid cartilage)	AMSBIO	Cat#400678-1A
Heparan Sulfate sodium salt (bovine kidney)	Sigma	Cat#H7640
Heparin-biotin sodium salt	Sigma	Cat#B9806
Heparinase I	AMSBIO	Cat#AMS.50-010
Heparinase III	AMSBIO	Cat#AMS.50-012-001
Heparinase I	Sigma	Cat#H2519, CAS: 9025-39-2
Heparinase III	Sigma	Cat#H8891, CAS: 37290-86-1
Chondroitinase ABC	Sigma	Cat#C3667
C3 transferase	Cytoskeleton	Cat#CT04
Biotin LC-Hydrazide	Thermo Fisher	Cat#21340
EDC (1-ethyl-3-(3-dimethylaminopropyl)carbodiimide hydrochloride)	Thermo Fisher	Cat#22980
JTE-013	Tocris	Cat#2392, CAS: 547756-93-4
Y-27632	Sigma	Cat#Y0503, CAS: 129830-38-2

(*Continued on next page*)

Continued

REAGENT or RESOURCE	SOURCE	IDENTIFIER
Critical Commercial Assays		
Amine Reactive Protein labelling kit RED	Nano Temper technologies	Cat#L001
Rhotekin-RBD beads	Cytoskeleton	Cat#RT02
RhoA G-LISA Activation Assay Kit	Cytoskeleton	Cat#BK124
Total RhoA ELISA	Cytoskeleton	Cat#BK150
Experimental Models: Cell Lines		
Cricetulus griseus: CHO K1 (WT)	ATCC	Cat#CCL-61
Cricetulus griseus: CHO pgsD-677	ATCC	Cat#CRL-2244
Homo sapiens: HEK293T	ATCC	Cat#CRL-3216
Mus musculus: Mouse WT embryonic fibroblasts	Kempf et al., 2014	N/A
Mus musculus: Mouse S1PR2$^{-/-}$ embryonic fibroblasts	Kempf et al., 2014	N/A
Mus musculus: Swiss 3T3	ATCC	Cat#CCL-92
Experimental Models: Organisms/Strains		
Mus musculus: C57/BL6	The Jackson Laboratory	Cat#000664
Mus musculus: S1PR2$^{-/-}$ (B6.129S6-S1pr2tm1Rlp) backcrossed into C57BL/6 background	Kono et al., 2004; Kempf et al., 2014	N/A
Rattus norvegicus: Sprague Dawley	Charles River	Cat#400
Rattus norvegicus: Wistar	Charles River	Cat#003
Oligonucleotides		
ON-TARGETplus SMARTpool rat Sdc3 siRNA	Dharmacon	Cat#L-098896-02-0005
ON-TARGETplus siRNA non-targeting pool	Dharmacon	Cat#D-001810-10-0005
Primer: mouse Gapdh_FWD: CAGCAATGCATCCTGCACC	This paper	N/A
Primer: mouse Gapdh_FWD: TGGACTGTGGTCATGAGCCC	This paper	N/A
Primer: mouse Rpl19_FWD: TGAGTATGCTCAGGCTACAG	This paper	N/A
Primer: mouse Rpl19_REV: GAATGGACAGTCACAGGCTT	This paper	N/A
Primer: mouse Sdc4_FWD: TTCTGGAGATCTGGATGACAC	This paper	N/A
Primer: mouse Sdc4_REV: CACCAAGGGCTCAATCAC	This paper	N/A
Primer: rat Gapdh_FWD: CTCTCTGCTCCTCCCTGTTC	This paper	N/A
Primer: rat Gapdh_REV: GCCAAATCCGTTCACACC	This paper	N/A
Primer: rat eF1_FWD: GCCACCATACAGTCAGAAGAG	This paper	N/A
Primer: rat eF1_REV: GAACCACGGCATATTAGCAC	This paper	N/A
Primer: rat Sdc3_FWD: TCCACGACAATGCCATCGACTC	This paper	N/A
Primer: rat Sdc3_REV: ACCTACGATCACAGCTACGAGCAC	This paper	N/A
Recombinant DNA		
MISSION mouse Sdc4 shRNA Plasmid DNA	Sigma	Cat#SHCLND-, Clone ID: -99s21c1
Mission shRNA TRC2 control Plasmid DNA	Sigma	Cat#SHC202
Mouse Ext1 cDNA	Wei et al., 2000	Accession No: NM_010162
pcDNA5/FRT Plasmid DNA	Invitrogen	Cat#V601020

CONTACT FOR REAGENT AND RESOURCE SHARING

Further information and requests for resources and reagents should be directed to and will be fulfilled by the Lead Contact, Anissa Kempf (anissa.kempf@cncb.ox.ac.uk).

EXPERIMENTAL MODEL AND SUBJECT DETAILS

Tissue extractions and animal experiments were performed in accordance with the guidelines of the Veterinary Office of the Canton of Zurich.

Primary Neuronal Cultures and Explants

Postnatal day 5-8 (P5-8) mouse cerebellar granule neurons (CGNs), P5-8 mouse dorsal root ganglia (DRG) neurons and embryonic day 19 (E19) rat cortical neurons were maintained in Neurobasal-A medium (GIBCO) supplemented with GlutaMAX (GIBCO), Penicillin/Streptomycin (Pen/Strep) (1x; GIBCO), B-27 (1x; GIBCO) and 10% FBS (Invitrogen). Mouse CGNs and DRGs were prepared from C57/BL6 mice pups. Rat cortical neurons were prepared from Wistar rat embryos.

Mouse P5 neuroblast explants were prepared from C57/BL6 mice pups. Tissues from the SVZ and RMS were embedded in 75% Matrigel growth factor reduced (BD Biosciences) and maintained in Neurobasal medium (GIBCO) supplemented with Glutamine (0.5 mM; Invitrogen), Pen/Strep (20 U/ml; Sigma) and B-27 (1x; Miltenyi).

SVZ cells were dissociated from adult C57/BL6 mice SVZs and maintained in DMEM/F-12 (GIBCO) supplemented with B-27 (1x; Miltenyi).

All primary cells were cultured at 37°C and 5% CO_2.

Cell Lines

Swiss 3T3 (ATCC) cells and primary mouse embryonic fibroblasts (MEFs) were maintained in Dulbecco's Modified Eagle medium (DMEM) (GIBCO) containing 10% neonatal calf serum (Invitrogen). MEFs were prepared from S1PR2$^{-/-}$ or littermate wild-type (WT) E14-E16 embryos. CHO K1 WT (ATCC) and CHO pgsD-677 cells (ATCC) were maintained in DMEM containing 10% fetal bovine serum (FBS) (Invitrogen). HEK293T (ATCC) cells were maintained in Iscove's Modified Dulbecco's medium (IMDM) (Life Technologies) supplemented with 4 mM L-Glutamine (Sigma), 1% Pen/Strep (GIBCO) and 10% FBS (Invitrogen).

All cell lines were cultured at 37°C and 5% CO_2.

METHOD DETAIL

Constructs and Protein Expression

BL21/DE3 *E. coli* were transformed with the pET28 expression vector (Novagen) containing His-/T7-tagged Nogo-A-Δ20 (rat aa 544-725), His-/T7-tagged Nogo-A-Δ21 (rat aa 812-918) or His-/HA-tagged Nogo-A-Δ20 (Oertle et al., 2003). Bacteria were cultured at 37°C to reach an OD of 0.6 AU. Protein expression was induced by addition of 1 M IPTG for 2 h at 30°C. Fusion proteins were purified using Co^{2+}-Talon Metal Affinity Resin (Takara Bio Inc.).

Brain-Derived Glycosaminoglycans (GAGs)

Adult Sprague Dawley rats were sacrificed and decapitated. The brains were cut into smaller pieces before de-lipidation with cold acetone. The tissues were then dried and homogenized in cold pronase buffer. The brain was then treated with pronase overnight and the proteins/peptides were removed by precipitation using trichloroacetic acid, followed by centrifugation. The residual trichloroacetic acid retained in the supernatant (which contains the GAGs) was removed with 5 diethyl ether washes. The GAGs were precipitated with sodium acetate and absolute ethanol overnight at 4°C and recovered after centrifugation. The resulting pellet was reconstituted in 500 μl of de-ionized water and stored at -20°C.

Spinal Cord Protein Extracts

One adult Wister rat was sacrificed and decapitated. The spinal cord was dissected and immediately homogenized using ice-cold extraction buffer (3.7% CHAPS, 20 mM Tris pH 8.0, 1 mM EDTA, 100 mM PMSF) containing protease inhibitors (EDTA-free Complete Mini, Roche). Homogenized tissue was incubated for 30 min on ice and ultracentrifuged at 170'000g for 1 h at 4 °C. Supernatant was aliquoted and snap-frozen in liquid nitrogen. The concentration was determined using a Bradford assay.

MEF Isolation

Primary WT and S1PR2$^{-/-}$ MEFs were prepared from E14-E16 embryos. The mother was sacrificed by cervical dislocation and embryos were isolated. Heads and dark organs were removed and used for genotyping. The rest of the embryos was cut into small pieces and enzymatically digested using 0.05% Trypsin/EDTA (Thermo Fisher Scientific). Post-digestion, the tissue was resuspended in DMEM and pipetted through a 40 μM filter to obtain single cells. MEFs were expanded and frozen.

Immunocytochemistry

Cell Lines and primary cells were fixed with 4% paraformaldehyde (PFA) for 15 min, washed and permeabilized with 0.1% Triton X-100. After blocking with 2% goat serum (Invitrogen), cells were first incubated with the primary antibodies for 30 min at room temperature and detected using corresponding secondary antibodies in 2% goat serum.

For cell-surface immunocytochemical detection of Nogo-A-Δ20, cells were first incubated with 1 μM HA-tagged Nogo-A-Δ20 and subsequently with anti-HA antibodies for 1 h each on ice in serum-free medium containing 0.02% sodium azide (Sigma). Cells were washed, fixed with 1% PFA and stained with secondary antibodies. Image stacks were acquired using a Leica SP5 confocal microscope equipped with a 63x oil immersion objective (NA 1.4). Stacks were reconstructed in 3D with Imaris (Bitplane) and the cell-surface area was measured for each cell. Bound Nogo-A-Δ20 puncta were counted using the spot function of Imaris and the total number was normalized to the cell-surface area for each cell. The average ratio obtained with secondary antibody only controls was baseline-subtracted from each cell.

Flow Cytometry

For FACS analysis, non-fixed cells were detached using 0.05% Trypsin/EDTA (Invitrogen), washed 1x in PBS, washed 2x in Tris-Buffer/1%BSA at 4°C and stained with the indicated primary antibodies followed by fluorescently-conjugated secondary antibodies for 30 min each in Tris-Buffer/5% BSA on ice. Cells were immediately analyzed by FACS (BD Canto II). FACS staining was quantitated using the FlowJo (Tree Star Inc) software. The fluorescence intensity is displayed on the X-axis (divided into 256 bins). The % of Max on the Y-axis represents the number of cells in each bin on the X-axis (FlowJo uses an arbitrary number of 256 bins) divided by the number of cells in the bin that contains the largest number of cells.

RhoA Activation Assays

3T3 cells were serum-starved overnight and treated for 20 min with 1 μM Nogo-A-Δ20 or Nogo-A-Δ21 control protein. Pulldown of activated RhoA-GTP was subsequently performed using the RhoA Activation Assay Biochem Kit according to the manufacturer's instructions (Cytoskeleton, Inc.). Alternatively, RhoA activation was assessed using the total RhoA ELISA and RhoA G-LISA kit according to the manufacturer's instructions (Cytoskeleton, Inc.). Levels of activated RhoA were normalized to total RhoA levels for each biological replicate.

Generation of Stable Cell Lines

Mission shRNA (Sigma) pLKO lentiviral plasmids containing shRNA against mouse syndecan-4 (TRCN0000331554) and non-target shRNA (SHC202 (TRC2 vector)) were transfected into HEK293T cells using PEI (polyethyleimine) 25 kDa (Polysciences Inc.). Lentiviruses were concentrated from filtered culture media by ultracentrifugation at 25000 rpm for 2 h. Swiss 3T3 cells stably expressing ctrl shRNA and Sdc4 shRNA were selected with 4 μg/mL puromycin. Quantification of the respective mRNA knockdown was performed by qRT-PCR.

Cell Spreading and Neurite Outgrowth Assays

Swiss 3T3 fibroblast spreading assays and neurite outgrowth assays were performed as follows. 4-well plates (Greiner) were coated with 40-100 pmol/cm^2 (0.4-1 μM) Nogo-A-Δ20 or Nogo-A-Δ21 (control protein) or 5 μg/cm^2 myelin at 4°C overnight. In outgrowth experiments, wells were precoated with 0.3 μg/ml Poly-L-Lysine (PLL; Sigma) for 1 h at 37°C before the addition of the different substrates. Unbound material was removed by 3 washes with PBS.

Cell lines were detached with 2% (w/v) EDTA (Invitrogen) in PBS and plated at 7000 cells per cm^2 for 1 h, fixed with 4% PFA and stained with Phalloidin-Alexa488. For HepI and HepIII (Sigma) treatment, cells were incubated with 2.5 U/ml HepIII or 2.5-10 U/ml HepI 3 h prior to plating and during the spreading assay. Higher concentrations of HepIII could not be used under our experimental conditions because of their effects on cell viability. For JTE-013 (Tocris), Y-27632 (Sigma) and cell-permeable C3 transferase (CT04, Cytoskeleton), cells were incubated with 1 μM JTE-013, 5 μM Y-27632 or 100 μg/ml C3 30 min prior to plating and during the spreading assay. The corresponding solvents or isotype antibodies were used as controls. For expression of EXT1 in pgsD-677 cells, pgsD-677 cells were transfected with pcDNA5-Ext1 or mock-transfected with pcDNA5(-) using Lipofectamine 2000 (Invitrogen) according to the manufacturer's instructions 48 h prior to replating. For shRNA experiments, Swiss 3T3 cells stably expressing ctrl and Sdc4 shRNA were plated onto Nogo-A-Δ20 or Nogo-A-Δ21 substrates in the presence of 4 μg/mL puromycin.

The percentage of cells that remained round, i.e. did not spread, was quantified manually in four randomly chosen areas of the well/coverslip and averaged over those areas (n = 1 coverslip). Data of all coverslips were normalized to the control values of coverslip #1 in experiment #1 and plotted as mean ± SEM from multiple coverslips.

CGNs were plated at 7.5x10^4 cells per cm^2, DRGs at 7.5x10^3 cells per cm^2 and cortical neurons at 5x10^4 cells per cm^2 onto the various substrates. Neurons were fixed with 4% PFA and stained with anti-βIII Tubulin (CGNs and DRGs) or Mab1b (cortical neurons). Treatment of CGNs with 500 mU/ml HepIII and DRGs with 1 U/ml HepIII started 12 h post-plating for 24 h. Cortical neurons were treated at DIV4 with 1 U/ml HepIII for 3 h and replated for 24 h in the presence of HepIII. The corresponding solvents were used as control. For siRNA experiments, E19 rat cortical neurons were plated at 0.6x10^6 cells in 6-well plates coated with 0.3 mg PLL and transfected at DIV4 with 50 nM siRNA using DharmaFECT 3 (Dharmacon) according to the manufacturer's instructions. 3 days post-transfection, neurons were detached with 0.25% Trypsin and replated on a Nogo-A-Δ20 or control substrate for 24 h.

Neurons were imaged with an Axioskop 2 microscope (Zeiss) equipped with a Plan-NEOFLUAR 10X/NA 0.3 objective in a semi-automated procedure. Mean total neurite length per cell was quantified using the MetaMorph software (Molecular Devices) in four randomly chosen areas of the well/coverslip and averaged over those areas (n = 1 coverslip). Data of all coverslips were normalized to the control values of coverslip #1 in experiment #1 and plotted as mean ± SEM from multiple coverslips.

Quantitative Real-Time PCR (qRT-PCR)

Total RNA was isolated with the RNeasy Micro kit (Qiagen) and reverse-transcribed using TacMan Reverse Transcription Reagents (Applied Biosystems). cDNA was amplified using the Light Cycler 480 thermocycler (Roche) with the polymerase ready mix (SYBR Green I Master, Roche). Relative quantification was performed using the comparative CT method. cDNA levels were normalized to the reference genes Gapdh and Rpl19 (mouse) or Gapdh and eF1a1 (rat). Each reaction was completed in triplicate. Melting curve analysis of PCR products followed by gel electrophoresis was performed to verify amplicons.

ELISA

The ELISA was modified according to the method described in (Purushothaman et al., 2007). Biotinylated GAGs (0.5 μg per well) were immobilized onto a streptavidin-coated 384-well-plate (Pierce/Thermo scientific). Biotinylation of GAGs was performed by EDC and biotin-LC-hydrazide conjugation (Pierce/Thermo Scientific). After biotinylated GAGs were immobilized on the plates, the plates were blocked in 1% BSA and subjected to the binding of recombinant Nogo-66-Fc, Nogo-A-Δ20-T7 or Nogo-A-Δ21-T7. The bound Nogo variants were then recognized by the anti-T7, anti-Fc or 11C7 antibodies. The bound antibodies were detected using anti-mouse-alkaline phosphatase conjugated antibodies followed by a direct measurement of absorbance at 405 nm using p-nitrophenylphosphate (Sigma Aldrich). BSA only control (no recombinant proteins) measurements were used as baseline in every experiment and subtracted from the other readings. For quantification, the mean ± SEM of absorbance measurements was determined from three experiments.

Explant Assay

Antibodies and compounds were mixed with Matrigel: 11c7 (Oertle et al., 2003), 1 μg/μl; mouse anti-human IgG, 1 μg/μl (Jackson ImmunoResearch); HepIII, 500 mU/ml (Sigma); JTE-013, 250 nM, 500 nM or 2 μM (Tocris). Only vital explants with cells moving out of the tissue core in chains were analyzed. Explants were fixed in 4% PFA for 40 min and stained using DAPI to visualize cell nuclei or labeled using βIII Tubulin or Doublecortin antibodies (Rolando et al., 2012) to mark neuroblasts. Migration data were normalized to the control group for each experiment and plotted as mean ± SEM from multiple experiments.

Adhesion Assay

SVZ-cells were either plated on poly-D-lysine (PDL) only or Nogo-A–Δ20-coated coverslips (12,000 cells/cm^2) (Rolando et al., 2012). Glass coverslips (1cm^2) were first coated with PDL (5 μg/ml) and then with Nogo-A–Δ20 (100 pmol/cm^2). Cells were pre-incubated with HepIII and/or 11c7 or with JTE-013 for 30 min and subsequently plated for 1 h. Cells were fixed, stained with DAPI and for βIII Tubulin and scored. The average number of adhered cells was determined by counting in five randomly chosen fields of view of the coverslips. Data of all coverslips were normalized to the control values of coverslip #1 in experiment #1 and plotted as mean ± SEM from multiple coverslips.

Microscale Thermophoresis

Microscale thermophoresis ligand binding measurements were performed using a Nanotemper Monolith NT.115 (Nano Temper technologies) (Wienken et al., 2010; Zillner et al., 2012). Recombinant Nogo-A–Δ20 was fluorescently labelled using the Amine Reactive Protein labelling kit, RED. A constant concentration of Nogo-A–Δ20 (40nM) was incubated with the different serially diluted recombinant proteins in PBS containing 0.025% Tween-20 at pH 7.4. 3-5 μl of each sample was loaded into a hydrophilic glass capillary (Nano Temper technologies) and thermophoresis analysis was performed (LED 60%, IR laser 20%) (Wienken et al., 2010; Zillner et al., 2012). MST data were normalized for baseline differences between 3 runs and K_d values were calculated using nonlinear regression assuming a Hill coefficient of 1.0 (GraphPad Prism).

QUANTIFICATION AND STATISTICAL ANALYSIS

Statistical analyses were conducted using the statistical software GraphPad Prism 5 or 6 (GraphPad Software Inc.). *$p < 0.05$ was considered statistically significant. Calculations were corrected for multiple comparisons as specified in the figure legends.